NANO LETTERS

Subscriber access provided by STANFORD UNIV GREEN LIBR

Letter

Void Formation Induced Electrical Switching in Phase-Change Nanowires

Stefan Meister, David T. Schoen, Mark A. Topinka, Andrew M. Minor, and Yi Cui

Nano Lett., **2008**, 8 (12), 4562-4567 • Publication Date (Web): 31 October 2008

Downloaded from http://pubs.acs.org on December 11, 2008

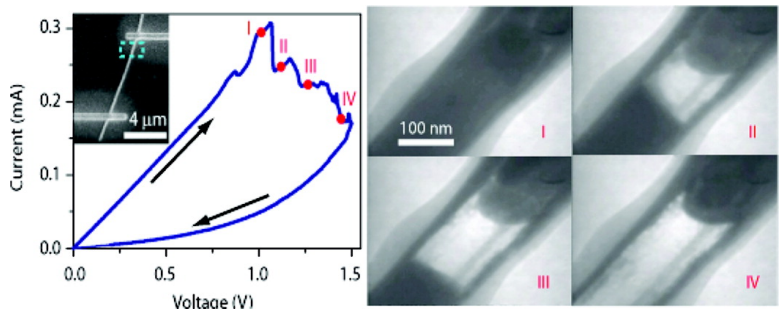

More About This Article

Additional resources and features associated with this article are available within the HTML version:

- Supporting Information
- Access to high resolution figures
- Links to articles and content related to this article
- Copyright permission to reproduce figures and/or text from this article

View the Full Text HTML

ACS Publications
High quality. High impact.

Nano Letters is published by the American Chemical Society. 1155 Sixteenth Street N.W., Washington, DC 20036

NANO LETTERS

2008
Vol. 8, No. 12
4562-4567

Void Formation Induced Electrical Switching in Phase-Change Nanowires

Stefan Meister,[†,‡] David T. Schoen,[†,‡] Mark A. Topinka,[§] Andrew M. Minor,[⊥] and Yi Cui*[,‡]

Department of Materials Science and Engineering, Department of Physics, Stanford University, Stanford, California 94305, National Center for Electron Microscopy, Lawrence Berkeley National Laboratory, and Department of Materials Science and Engineering, University of California, Berkeley, California 94720

Received September 16, 2008

ABSTRACT

Solid-state structural transformation coupled with an electronic property change is an important mechanism for nonvolatile information storage technologies, such as phase-change memories. Here we exploit phase-change GeTe single-nanowire devices combined with ex situ and in situ transmission electron microscopy to correlate directly nanoscale structural transformations with electrical switching and discover surprising results. Instead of crystalline-amorphous transformation, the dominant switching mechanism during multiple cycling appears to be the opening and closing of voids in the nanowires due to material migration, which offers a new mechanism for memory. During switching, composition change and the formation of banded structural defects are observed in addition to the expected crystal-amorphous transformation. Our method and results are important to phase-change memories specifically, but also to any device whose operation relies on a small scale structural transformation.

Over the past several years, phase-change memory (PCM) has become a promising candidate as a flash replacement because of its excellent scalability,[1,2] high-speed switching, long lifetime, and nonvolatility.[3] PCM operates by reversibly driving a small volume of material through a reversible crystal-amorphous structural transition. The phase-change is actuated electrically by joule heating, and the two states can be easily distinguished due to the substantially lower resistivity of the crystalline phase compared to the amorphous one. Recent theoretical and experimental studies have provided great insight toward the understanding of the atomistic mechanism involved.[4−11] Cells usually have a vertical architecture, where the PCM material is sandwiched between two electrodes.[12] This structure can be integrated into a CMOS architecture. However, vertical cells do suffer from one significant drawback for fundamental study. Since the active material is buried inside of several other materials, it is extremely difficult to directly probe the structural transformation inside a working device. Efforts have been made to examine these vertical cells by cutting cross sections of working devices with a focused ion beam (FIB), but so far there are no reports of reversible switching in such cross sectioned devices, preventing in situ observation of the phase transformation.

Cells have also been fabricated in a horizontal architecture, where the PCM material is fabricated into a narrow bridge between two electrodes.[13,14] This open structure is much more amenable to characterization. The bridge is not buried under an electrode, so it is accessible from above with probe microscopy. A careful choice of substrate[15] can allow even for direct observation of the structure in a transmission electron microscope (TEM). PCM nanowires (NWs) developed recently by our group[16] and others[17−19] are good candidates to be used as the active material in horizontal line cell studies. NWs present several advantages over patterned thin films: They have smooth well-defined surfaces, they are initially in a high quality single crystalline state, and they can be deposited on a substrate in a single solvent-free room temperature step.[15] Single crystalline GeTe NWs are particularly interesting, because their diameter is smaller than grains in crystallized thin films that are on the order of several micrometers.[20] The electrical switching properties of single NWs have been studied and excellent scaling behaviors have been shown,[18,21] but so far little work has been done that takes advantage of the horizontal architecture of NW devices for in depth characterization of the details of the structural transformation. Of particular interest are the size and location of the amorphous domains of the devices in the off state, the growth morphology and kinetics of the

* To whom correspondence should be addressed. E-mail: yicui@stanford.edu.
[†] These authors contributed equally to the work.
[‡] Department of Materials Science and Engineering.
[§] Department of Physics, Stanford University.
[⊥] University of California.

10.1021/nl802808f CCC: $40.75 © 2008 American Chemical Society
Published on Web 10/31/2008

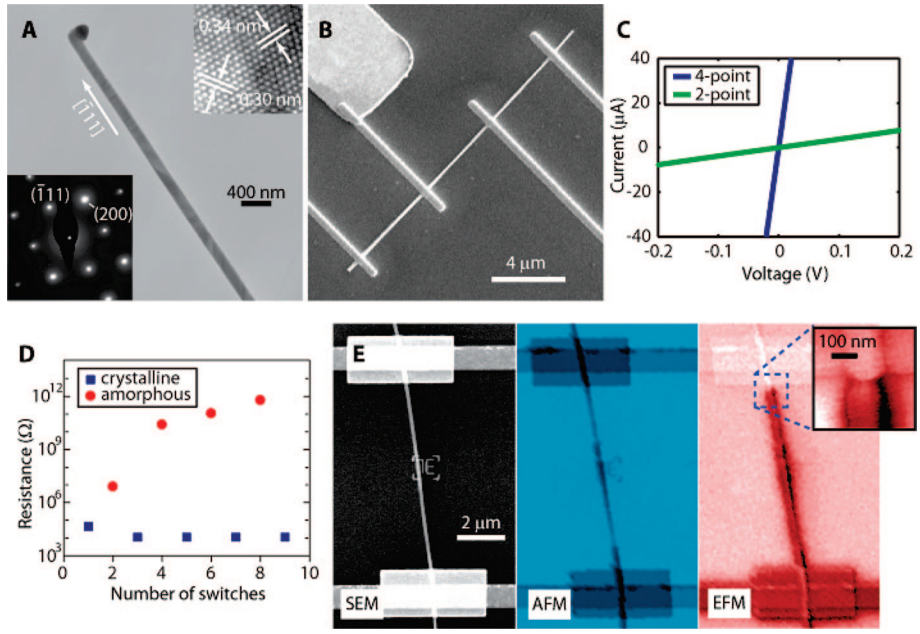

Figure 1. (A) TEM image of GeTe nanowire with a [-1 1 1] growth direction. SAED and HRTEM (inset). (B) GeTe nanowires with four platinum contacts fabricated by FIB. (C) Four-point and two-point IV measurement of device in panel B revealing significant contact resistance. (D) Cycling behavior. Nanowires were switched to a high resistance state with a 10 V, 200 ns pulse, and back to the low resistance state with a 100 mV/s scan up to 5 V. (E) SEM, AFM, and EFM images of the same single nanowire device in a high resistance state. There is a 2 V difference between the light and dark color in the EFM image.

crystalline domains when switching to the on state, and any other behaviors that may limit device reliability or dictate the power needed to actuate the devices.

In order to answer some of these questions we grew single crystal GeTe NWs and have fabricated a large variety of devices on NWs ranging in diameter from 60 to 200 nm. Our as-grown NWs are single crystalline with the equilibrium rhombohedral phase of GeTe (Figure 1A). Figure 1B shows an SEM image of a NW with four Pt contacts on Si-SiO_2 substrate. Two-point and four-point probe measurements show a linear behavior; however, the lower resistance obtained by the four-point probe measurement reveals that even in the crystalline state, the majority of the resistance comes from the contacts (Figure 1C). The two-point probe resistance of 26 kΩ is ∼50 times higher than the four-point resistance of 530 Ω, suggesting that the contact resistance is much larger than the intrinsic NW resistance. The resistivity of the NWs as calculated from the 4-point measurement is approximately 4×10^{-4} Ω•cm, which is consistent with the bulk value of GeTe.[22] Our measurements conducted on approximately 50 devices show that the contact resistance is 5−50 times that of the NW resistance. Occasionally, the contact resistance is similar to the NW resistance. We believe that the contact resistance is in part due to the existence of an amorphous oxide layer between metal leads and NWs.[23]

The NWs can be switched from a low resistance to a high resistance state by applying a short voltage pulse, as in previous studies.[17,21] Despite an intrinsic, amorphous germanium oxide of 2−5 nm thickness on the NW surface, switching back to the low resistance state was not observed unless the NWs were coated in an extra encapsulation layer. For our study, we sputtered 20 nm SiO_2 on to the completed devices. Figure 1D shows the resistance as a function of switching cycles for a NW that is 200 nm in diameter and 5 μm in length encapsulated with 20 nm of SiO_2. The NW with an initially low two-point resistance state of 44 kΩ switches to a high two-point resistance state of 8 MΩ after applying a short (200 ns) voltage pulse with 10 V amplitude. Switching back to the low-resistance was accomplished by a voltage scan to 5 V at a rate of 100 mV/second. There are several interesting observations. First, the resistance of the device in the on state drops slightly from the initial on state after the first cycle. This can probably be explained by annealing of the contacts by joule heating leading to a lower contact resistance. Second, since the resistivity in the crystalline state after the first cycle is 11 kΩ, the following 10 V pulses correspond to approximately 0.9 mA of current (or a current density of 2.9×10^6A/cm^2), which is 4 times lower than previously reported values for a 100 ns pulse.[21] Lastly, and most significantly, the on−off ratio of our NW devices after the first cycle is increased with cycling to nearly 10^7. While this ratio is similar to what has been found in thin film studies,[24] a previous NW study has revealed a rather large diversity of values for the on−off ratio,[17] from 10^3 to 10^7, and our values are at the top of this range.

A naïve model for the resistivity of the off state might simply take into account the volume of transformed material. If a cylindrical plug of the NW is transformed to the amorphous state, one would expect the resistance to scale linearly with the length of this plug. Given that the value of the resistivity of the amorphous phase is between 10^3 and 10^4 Ω•cm,[22,24] in order to measure a resistance of 100 GΩ in a roughly cylindrical wire of diameter 200 nm, the wire would have to be more than 30 μm long even taking the lower value for the reported resistivity. This observation is

interesting, because our devices have an electrode separation less than 10 μm. Even though the resistivity of the amorphous GeTe devices in our NWs may be somewhat different than that reported for the thin films, one would assume that at least the entire device under measurement must transform to the amorphous phase to generate the measured resistance. In order to test this prediction, devices switched to a highly resistive state were examined via electric force microscopy (EFM). Figure 1E shows three different images of a device taken with scanning electron microscopy (SEM), atomic force microscopy (AFM), and EFM (from left to right). The contrast in the EFM image is due to the local electric potential and topographic features. If the whole NW had transformed to the amorphous phase as expected, the EFM should show a gradual change in contrast from one contact to the other as the potential slowly drops through the uniformly resistive region. The observation in Figure 1E is quite different however as the entire voltage appears to drop over a region tightly confined to the top contact, suggesting that the structural transformation is localized there, contrary to the expectation based on the naïve model and the measured switching data.

This inconsistency provided the motivation necessary to fabricate the NW devices on electron transparent silicon nitride membranes (Figure 2A), making possible direct observation of the NWs' structure by TEM[25] in the high and low resistance state. Our initial work focused on discovering the structure of the off state after pulse induced switching in air. During TEM observation, care was taken to avoid e-beam induced damage. The bottom left inset of Figure 2B shows a TEM image of a NW device before switching. The initial two-point resistance was 8 kΩ. The NW was very stable with respect to 200 ns square pulses with voltage below 10 V. After a 10 V pulse in air, which resulted in a current of approximately 1.3 mA, the two-probe resistance was changed to 10^{12} Ω. Interestingly, a dramatic structural change was observed close to one of the contacts (bright contrast in NW, Figure 2B (main panel and inset)). The structure observed is a thin amorphous hollow tube of GeO_x confirmed by EDS, indicating a void formed in the NW. GeO_x is highly resistive and even a small segment close to the metal contact can increase the measured NW resistance up to 10^{12} Ω, suggesting that this void formation can be a switching mechanism for the devices.

Considerable effort was invested to apply pulses just large enough to raise the resistance of the NWs without forming voids. A 20 μs voltage pulse of 3.5 V on a device with a large electrode separation of 15 μm and resistivity of 12 kΩ, results in very little change. Only some hillock formation and small pinholes are observed (Supporting Information, Figure S1). When the pulse is raised to 4.0 V, the resistance is increased by 10^4 to 100 MΩ and a surprising variety of structural transformations are observed (Figure 2C). Bulging and small voids are formed as before, but we also observe a periodic set of planar defects in one section of the NW (Figure 2D) that extends over several microns. These defects are likely twin boundaries formed by cooling GeTe from its higher temperature cubic phase back to the room temperature

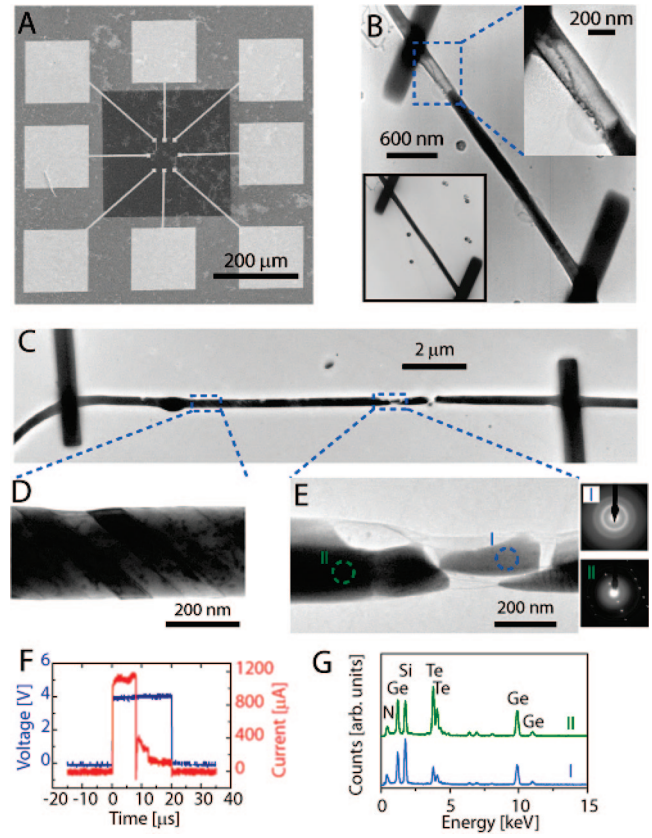

Figure 2. (A) Low-magnification SEM image of a silicon nitride membrane (dark) with gold contact pads (light). (B) Nanowire before (lower left inset) and after pulsing (main panel); the switching mechanism is identified as void formation at the top contact (upper right inset). (C) TEM low-magnification image of nanowire after a long low magnitude pulse. (D) Banded planar defect structure. (E) Void and amorphous region formation. Area I is amorphous and II, like the rest of the wire, is crystalline (SAED inset). (F) Pulse applied to NW in panel C. Blue is the applied voltage, and red is the current through the device. (G) EDS spectrum of areas I and II from part E.

rhombohedral phase[26] and can also be epitaxial misfit upon regrowth of material with different compositions. Further studies are required to clarify these details. A region that was transformed to the amorphous state was also observed (Figure 2E); its structure was confirmed by selected area electron diffraction of the slightly brighter area (amorphous, top inset) and the darker area (crystalline, bottom inset). The amorphous region has also undergone a composition change as shown in the comparative EDS spectrum in Figure 2G. The amorphous region has been partially depleted of tellurium, most likely due to the higher vapor pressure of tellurium at temperatures sufficient to melt the material. The tellurium may escape the GeO_x shell through small defects formed during the heating process, since no tellurium rich areas have been observed. It should be noted that in this case the transformations occurred over large parts of the NW, because its resistance during the pulse is similar to the contact resistance resulting in less localized heating. Figure 2F shows the voltage pulse and current response in the NW indicating an initial resistance of only 3.7 kΩ. These experiments illustrate dramatically the fundamental mechanisms that render reversible switching in these systems impossible

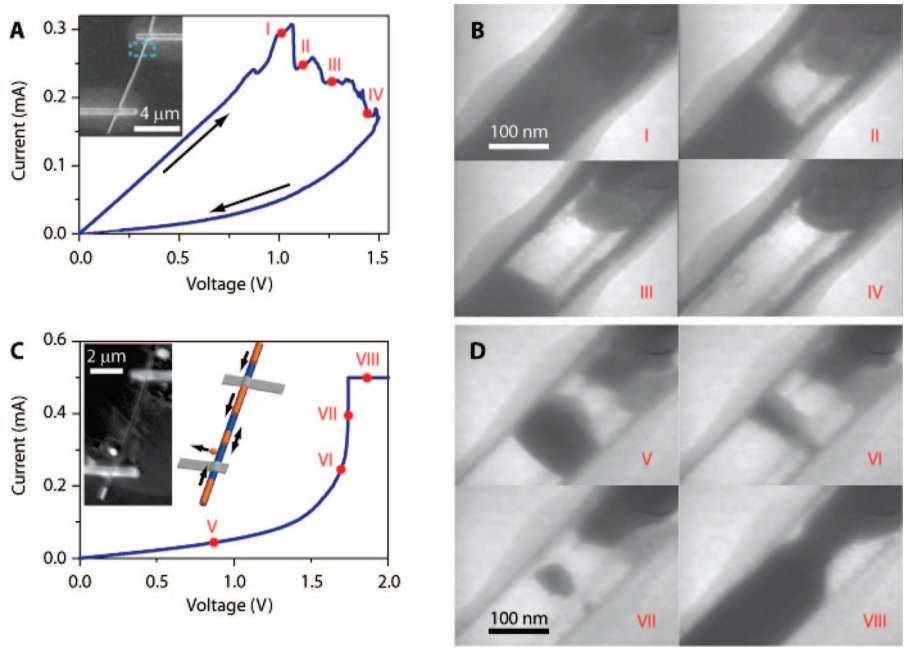

Figure 3. (A) Voltage scan on a single nanowires device (inset). The blue square in the inset shows the location of the TEM observation in panel B. (B) TEM images taken in situ during the voltage scan in panel, at times I, II, III, and IV. Note the correlation of resistance with void size. (C) Second voltage scan on the same wire showing switching to initial low resistance state. Inset displays an SEM image of the same NW after repeated pulsing and voltage scanning. On the NW, the dark contrast indicates the hollow tube and the bright contrast indicates the existence of GeTe materials; inset also shows a schematic of the material flow inside the NW. (D) In situ TEM images. At time VIII, the void is suddenly refilled and the current jumps past compliance in the voltage scan.

without a high quality encapsulating shell, but the large number of structural transformations observed in the ex situ study makes it very difficult to determine which structural transformation is chiefly responsible for the measured resistance change during reversible switching.

In order to determine which of the observed behaviors was primarily contributing to the resistance change, the dynamic behavior of the NWs was recorded as a real-time movie via in situ electron microscopy of the devices under a voltage scan (Supporting Information, Movie S1). Figure 3 summarizes the surprising results of such a measurement with a NW coated with 20 nm sputtered silicon oxide (Figure 3A inset). Parts A and B show the electrical and structural behavior of the NW beginning with its as fabricated condition with a low initial two-point resistance of 3.7 kΩ. Similarly to the ex situ observations, the initial increase in resistance between points I and II in Figure 3A is correlated with the formation of a small void. As more current is applied, the resistance of the device continues to rise, correlating with the growth of the void. A thin shell of GeTe material on the inside of the encapsulating oxide tube appears to be providing a current path through the device around the void. A blue rectangle shows where the initial structural changes happened due to the voltage scan as shown in Figure 3B. At the end of the scan the NW's resistance has increased to 42 kΩ (∼10 time the original resistance), and the void has grown to almost 1 μm in length. Similar opening of voids can also be achieved via pulsing the nanowire (Supporting Information, Movie S2), but there tends to be less GeTe remaining resulting in higher final resistances.

Remarkably, a new mechanism for returning the device to a low resistance state is observed (Figure 3C,D). At point V, the NW remains in a high resistance state, and large regions of void are observed by TEM. As the voltage is scanned past 1.5 V, movement in the remaining material is observed (Supporting Information, Movie S3). At points VI and VII, the TEM observation suggests that the material appears to have become molten, and at point VIII, the shell is suddenly refilled with material (Supporting Information, Movie S3). This closing of the void is correlated with a large increase in the measured current, carrying it over the compliance set for the measurement (Figure 3C). The final resistance measured is similar to the resistance of the NW in its original state before any void formation had been observed. Although it is a counter-intuitive conclusion, this void formation mechanism is the best candidate for explaining the extremely large on−off ratios observed in the many NW devices fabricated and tested on regular substrates. Examination of the NW by SEM after several cycles of this behavior is shown in the inset to Figure 3C, in which the bright (dark) contrast on the NW indicates the presence (absence) of GeTe materials. It can be plainly seen that material from outside the contacts appears also to have participated since part of the NW at outside appears to be empty (dark), revealing that the material in the NW outside the contacted region can be a source for refilling voids. A schematic (Figure 3C inset) illustrates the observed flow of material.

The exact mechanisms that lead to this movement of material are not yet understood, but one general observation across all the TEM studies has been that the observed structural transformations are localized to rather small regions of the NW. These regions are usually, but not always, located close to the contacts. A very simple analysis with com-

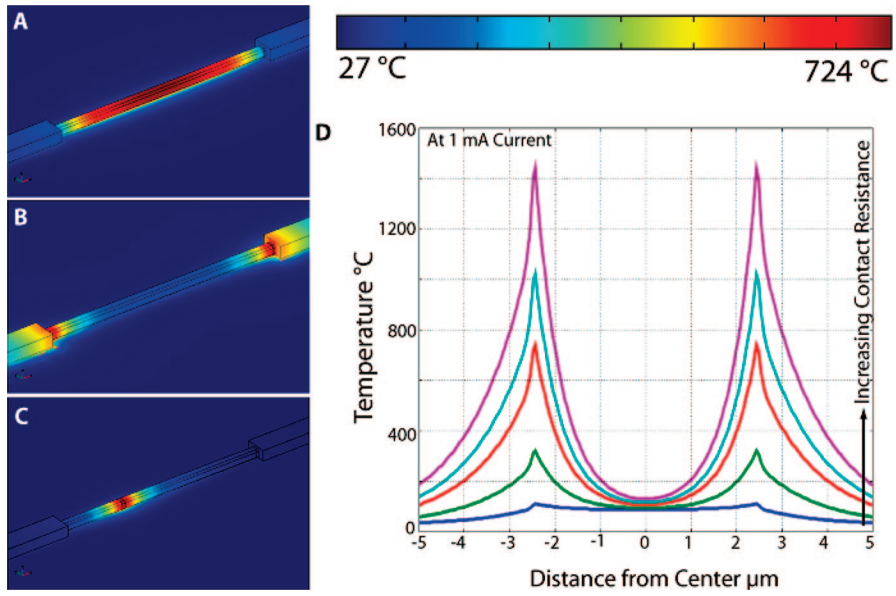

Figure 4. (A) Finite element simulation of a GeTe nanowire with no contact resistance. The color map is a plot of the temperature of the surface, the blue color is room temperature and the dark red is just above GeTe's melting point, 724 °C. To reach this temperature, 2V is required. (B) GeTe nanowire with 5 kΩ of resistance at each contact. Ten volts are applied, and the maximum temperature is 660 °C. (C) Nanowire with a 10 kΩ resistive region along the length. The maximum temperature is GeTe melting point, reached at 4.6 V. (D) Temperature line scan of a nanowire with 1 mA current for several values of the contact resistance. Total resistance is 1, 6, 10, 16, and 20 kΩ.

mercially available finite element software can reveal that these changes are most likely caused by a concentration of heat either at small resistive defects in the NW, such as necks formed after switching, or at the contacts due to the large contact resistance observed in most of the NW studies. Figure 4 shows the results of such a simulation of a NW contacted by two platinum electrodes on a Si-SiO_2 substrate as used in the experiments of Figure 1. The bulk values are used for all of the pertinent materials properties. If the contact resistance is neglected, the heating in the NW appears to be quite uniform (Figure 4A). When a contact resistance is included in the simulation (Figure 4B) the heating becomes strongly confined to the contact area. Figure 4D shows this effect for several different contact resistances for a nanowire subjected to 1 mA of current, which reveals that the temperature at the contact area can be several hundred °C higher than at the center of the NW. For a constant current, higher contact resistances also lead to higher temperatures. If the resistive area of the NW is instead located at some point along the length due to defects, such as a void, the heating is concentrated there (Figure 4C). Since the actual pattern of transformation in a NW can be very complicated and narrow regions can be observed to move, one might expect the heating during a voltage scan to be highly dynamic. Since voids can be observed to form on either or both of the positive and negative electrode after a pulse or scan, and material can be seen to move in either direction in the same NW during the same scan, electromigration can probably be ruled out as a dominant mechanism. Instead, expansion of material due to melting and pressure buildup in the oxide encapsulation due to the evaporation of tellurium seem the most likely candidates leading to the observed motion of liquid PCM material.

Materials and Methods. ***Instruments and Measurements.*** Platinum deposition was performed with an FEI Strata 235DB dual-beam FIB/SEM with a 10 pA Ga^+ ion beam and an accelerating voltage of 30 kV. Scanning electron microscope (SEM) images were obtained with the same FEI strata or an FEI XL30 Sirion SEM with FEG source. The EFM image was obtained with an Asylum MFP-3D AFM. The scan was performed in a noncontact mode at 200 nm tip−sample separation with one electrode grounded, the other electrode held at 2 V and the tip at −1 V. The ex situ TEM studies were carried out on an FEI CM20 operated at 200 kV, and the in situ TEM studies were carried out in a JEOL 3010 operated at 300 kV at the National Center for Electron Microscopy at Lawrence Berkeley National Laboratory.

Resistance measurements in the lower resistive states were done at a low bias of 0.2 V, the highly resistive states (R > 1 GΩ) were measured at a bias of 2 V.

Sample Preparation. Silicon nitride TEM membranes can be purchased directly (i.e., Structure Probe, Inc.) or fabricated via a KOH etch of a Silicon wafer with a low stress thin film of Silicon Nitride on the front and a patterned layer of Silicon Nitride acting as the etching mask on the back side of the wafer. We performed standard e-beam lithography (EBL) techniques to define the Au pads and electrodes that are shown as light squares and lines in the SEM image in Figure 2A. The darker inner square is the actual Silicon Nitride membrane. The larger Au pads allow us to make electrical contact with the tips of either a probe station or the prongs of the in situ TEM holder. The Au electrodes are deposited directly onto the 50 nm thin SiN_x. Nanowires were deposited by dry or wet transfer, specifically by touching the membrane to a silicon chip on which NWs were grown, or by dripping NWs suspended in isopropyl alcohol onto

the membrane, respectively. The NWs were synthesized by the vapor−liquid−solid mechanism grown at 450 °C for 4 h in Argon at a pressure of 10 Torr. Finally, contact to single nanowires is established via depositing Pt with a focused ion beam (FIB). To encapsulate the devices, a 20 nm Silicon Oxide was sputtered from a stoichiometric target.

Modeling. Simulations were carried out with COMSOL Multiphysics. The overall geometry can be seen in Supporting Information, Figure S3. The GeTe nanowire is 5 μm long and has an octagonal cross section of radius 200 nm. The contacts are platinum 5 μm in length, 250 nm thick, and 500 nm wide. They are contacted by gold pads 150 nm thick, 5 μm wide, and 3.25 μm long. They are sitting on a SiO_2 membrane 175 nm thick on top of a Si substrate 2 μm tall. Simulations presented were done with the overall dimensions as shown below; however, some simulations were run with much wider and deeper substrate simulation with no appreciable effect on the quantities of interest. All temperatures were initially set to 300 K. The sides and bottom of the substrate were fixed at 300 K, as were the two outside edges of the gold pads, while all other exterior surfaces were set as thermally insulating. Electrical behavior was simulated only in the gold, platinum, and GeTe materials, while the thermal behavior was simulated in the substrate as well. The properties used are given in Supporting Information, Table S1. In order to model the effect of contact resistance or a resistive defect, a small region 50 nm wide of the nanowire at each contact was set to a resistivity necessary to achieve some total desired contact resistance, given in the Figure 4B and 4D. For the defect these resistive regions were moved to a location along the NWs length as shown in Figure 4C.

Supporting Information Available: Figures S1, S2, S3, and Table S1. Movie S1. Closing and opening of gap during voltage scan. Movie S2. Opening of void due to 4V, 10 μs pulse. Movie S3. Closing of void during voltage scan as depicted in Figure 3C. This material is available free of charge via the Internet at http://pubs.acs.org.

References

(1) Hamann, H. F.; O'Boyle, M.; Martin, Y. C.; Rooks, M.; Wickramasinghe, K. *Nat. Mater.* **2006**, *5* (5), 383–387.
(2) Milliron, D. J.; Raoux, S.; Shelby, R.; Jordan-Sweet, J. *Nat. Mater.* **2007**, *6* (5), 352–356.
(3) Wuttig, M.; Yamada, N. *Nat. Mater.* **2007**, *6*, 824–832.
(4) Hegedus, J.; Elliott, S. R. *Nat. Mater.* **2008**, *7* (5), 399–405.
(5) Kolobov, A. V.; Fons, P.; Frenkel, A. I.; Ankudinov, A. L.; Tominaga, J.; Uruga, T. *Nat. Mater.* **2004**, *3* (10), 703–708.
(6) Kolobov, A. V.; Fons, P.; Tominaga, J.; Ankudinov, A. L.; Yannopoulos, S. N.; Andrikopoulos, K. S. *J. Phys.: Condens. Matter* **2004**, *16* (44), S5103−8.
(7) Welnic, W.; Pamungkas, A.; Detemple, R.; Steimer, C.; Blugel, S.; Wuttig, M. *Nat. Mater.* **2006**, *5* (1), 56–62.
(8) Sun, Z. M.; Zhou, J.; Ahuja, R. *Phys. Rev. Lett.* **2007**, *98* (5), 055505.
(9) Kohara, S.; Kato, K.; Kimura, S.; Tanaka,H.; Usuki, T.; Suzuya, K.; Tanaka, H.; Moritomo, Y.; Matsunaga, T.; Yamada, N.; Tanaka, Y.; Suematsu, H.; Takata, M. *Appl. Phys. Lett.* **2006**, *89* (20), 201910.
(10) Wuttig, M.; Lusebrink, D.; Wamwangi, D.; Welnic, W.; Gillessen, M.; Dronskowski, R. *Nat. Mater.* **2007**, *6* (2), 122–U7.
(11) Andrikopoulos, K. S.; Yannopoulos, S. N.; Voyiatzis, G. A.; Kolobov, A. V.; Ribes, M.; Tominaga, J. *J Phys: Condens. Matter* **2006**, *18* (3), 965–79.
(12) Hudgens, S.; Johnson, B. *MRS Bull.* **2004**, *29* (11), 829–832.
(13) Lankhorst, M. H. R.; Ketelaars, B.; Wolters, R. A. M. *Nat. Mater.* **2005**, *4* (4), 347–352.
(14) Chen, Y. Y. *Tech. Dig. - Int. Electron Devices Meet.* **2006**, *531*.
(15) Sedgwick, T. O.; Agule, B. J.; Broers, A. N. *J. Electrochem. Soc.* **1972**, *119* (12), 1769.
(16) Meister, S.; Peng, H.; McIlwrath, K.; Jarausch, K.; Zhang, X. F.; Cui, Y. *Nano Lett.* **2006**, *6* (7), 1514–1517.
(17) Yu, D.; Wu, J.; Gu, Q.; Park, H. *J. Am. Chem. Soc.* **2006**, *128* (25), 8148–8149.
(18) Lee, S. H.; Jung, Y.; Agarwal, R. *Nat. Nanotechnol.* **2007**, *2*, 626–630.
(19) Lee, J. S.; Brittman, S.; Yu, D.; Park, H. *J. Am. Chem. Soc.* **2008**, *130* (19), 6252–6258.
(20) Chopra, K. L.; Bahl, S. K. *J. Appl. Phys.* **1969**, *40* (10), 4171–4178.
(21) Lee, S. H.; Ko, D. K.; Jung, Y.; Agarwal, R. *Appl. Phys. Lett.* **2006**, *89*, (22), 223116.
(22) Mikolaichuk, A. G.; Kogut, A. N.; Ignativ, M. I. *Izv. Vyssh. Uchebn. Zaved., Fiz.* **1970**, (7), 103.
(23) Sun, X. H.; Yu, B.; Ng, G.; Meyyappan, M. *J. Phys. Chem. C* **2007**, *111* (6), 2421–2425.
(24) Bahl, S. K.; Chopra, K. L. *J. Appl. Phys.* **1970**, *41* (5), 2196.
(25) Peng, H.; Xie, C.; Schoen, D. T.; Cui, Y. *Nano Lett.* **2008**, *8* (5), 1511–1516.
(26) Stoemenos, J.; Vincent, R. *Phys. Status Solidi A* **1972**, *11* (2), 545–558.

NL802808F